nature neuroscience

Selective inhibitory control of pyramidal neuron ensembles and cortical subnetworks by chandelier cells

Jiangteng Lu[1,5], Jason Tucciarone[1,2,5], Nancy Padilla-Coreano[3], Miao He[1,4], Joshua A Gordon[3] & Z Josh Huang[1]

The neocortex comprises multiple information processing streams mediated by subsets of glutamatergic pyramidal cells (PCs) that receive diverse inputs and project to distinct targets. How GABAergic interneurons regulate the segregation and communication among intermingled PC subsets that contribute to separate brain networks remains unclear. Here we demonstrate that a subset of GABAergic chandelier cells (ChCs) in the prelimbic cortex, which innervate PCs at spike initiation site, selectively control PCs projecting to the basolateral amygdala ($_{BLA}$PC) compared to those projecting to contralateral cortex ($_{CC}$PC). These ChCs in turn receive preferential input from local and contralateral $_{CC}$PCs as opposed to $_{BLA}$PCs and BLA neurons (the prelimbic cortex–BLA network). Accordingly, optogenetic activation of ChCs rapidly suppresses $_{BLA}$PCs and BLA activity in freely behaving mice. Thus, the exquisite connectivity of ChCs not only mediates directional inhibition between local PC ensembles but may also shape communication hierarchies between global networks.

In many areas of the cerebral cortex, diverse and often intermingled subsets of PCs preferentially receive inputs from and project outputs to distinct brain areas, and thus are embedded in separate local circuits as well as global networks[1]. It is not well understood how specific physiological PC ensembles emerge from the underlying anatomic scaffold and contribute to different subnetworks and information processing streams. Diverse types of GABAergic interneurons appear to specialize in their inhibitory control of various aspects of cortical circuit operations, such as balancing excitation, modulating gain, tuning dynamics and generating oscillations[2–4]. However, the inhibitory mechanisms that regulate the dynamic segregation of functional PC ensembles and route information flow between brain networks remain elusive.

ChCs (i.e., axo-axonic cells) are among the most distinctive interneuron types. ChCs selectively innervate PCs at their axon initial segment (AIS), the site of action potential initiation[5]. A single ChC innervates hundreds of PCs[6,7], and multiple ChCs can converge onto the same PC[8,9]. The exquisite specificity of ChC innervation at the AIS has long been speculated to exert the ultimate inhibitory control over PC spiking and population output[10,11]. However, it remains unclear how ChCs are recruited and whether a ChC indiscriminately innervates PCs within its dense axonal arbor or selects a specific PC subset[9]. In fact, it is even controversial whether ChCs inhibit or excite PCs[12–14]. Thus the problem of how ChCs control PCs represents a prominent gap as well as a unique opportunity for understanding the cellular basis of cortical organization, which entails elucidating the connectivity pattern of ChCs to PC subsets within local circuits in the context of global brain networks.

Rodent prelimbic cortex (PL) integrates inputs from the amygdala and other brain structures (for example, other cortical areas, ventral hippocampus, medial-dorsal thalamus) to gate fear expression via projections back to the amygdala[15–19]. The superficial layers of PL contain two subsets of PCs: one projects to the BLA ($_{BLA}$PC) and another projects to contralateral cortex ($_{CC}$PC)[15,20]. They form two separate subnetworks: the PL–BLA network, comprising reciprocally connected $_{BLA}$PCs and BLA neurons, and the bilateral PL network, comprising $_{CC}$PCs from the two hemispheres[20]. Here, by combining genetic labeling of ChCs and projection-based labeling of PC subsets, we demonstrate that a subset of layer 2 (L2) ChCs preferentially receives inputs from $_{CC}$PCs yet selectively innervates $_{BLA}$PCs. This highly directional ChC microcircuit module is distinct from the parvalbumin fast-spiking basket cell (PVBC) module, characterized by nonselective and extensive reciprocal connectivity with $_{BLA}$PCs and $_{CC}$PCs. Transsynaptic rabies tracing combined with optogenetic tagging of long-range inputs further revealed that L2 ChCs are preferentially recruited by contralateral $_{CC}$PCs, but not by BLA input. Notably, optogenetic activation of ChCs resulted in rapid inhibition of PC firing in freely moving mice. Together, these results reveal that the exquisite connectivity of ChCs not only mediates directional inhibitory control between local PC ensembles but may also shape communication hierarchy and route information flow between distinct PC-associated global networks.

RESULTS

A subset of L2 ChCs selectively innervates $_{BLA}$PCs over $_{CC}$PCs in PL

We combined genetic[21] and anatomic methods to reliably label ChCs, $_{BLA}$PCs and $_{CC}$PCs for physiological studies. Tamoxifen induction in pregnant *Nkx2.1-CreER;Rosa26-loxpSTOPloxp-TdTomato* (*Ai14*) mice (where the *Nkx2.1* promoter is from Nkx2 homeobox 1, gene

[1]Cold Spring Harbor Laboratory, Cold Spring Harbor, New York, USA. [2]Program in Neuroscience and Medical Scientist Training Program, Stony Brook University, Stony Brook, New York, USA. [3]Departments of Neuroscience and Psychiatry, Columbia University, New York, New York, USA. [4]Present addresses: Institutes of Brain Science, State Key Laboratory of Medical Neurobiology, Collaborative Innovation Center for Brain Science, Fudan University, Shanghai, China (M.H.) and National Institute of Mental Health, Rockville, Maryland, USA (J.A.G.). [5]These authors contributed equally to this work. Correspondence should be addressed to Z.J.H. (huangj@cshl.edu).

Received 30 September 2016; accepted 17 July 2017; published online 21 August 2017; doi:10.1038/nn.4624

symbol *Nkx2-1*) at embryonic day 17.5 (E17.5) resulted in specific labeling of a subset of L2 ChCs throughout the frontal cortex, characterized by their soma positions at the L1–L2 border, prominent dendritic arborization in L1 and dense axonal plexus in L2/3 (**Fig. 1a**,**b** and **Supplementary Fig. 1**). It should be noted that L2 ChCs are also generated at earlier embryonic times[21]; for simplicity, the E17.5-born subset of L2 ChCs are herein referred to as L2 ChCs. Single-cell reconstruction revealed that individual L2 ChCs elaborated on average 211 ± 28 'cartridges', vertical strings of boutons targeting the AIS of PCs (**Fig. 1b** and **Supplementary Fig. 2**). We distinguished subpopulations of L2/3 PCs in PL according to their projection targets by injecting a different color of retrograde tracer cholera toxin subunit B (CTB) into each target region of the same mouse: the BLA (to label $_{BLA}$PCs), contralateral cortex (to label $_{CC}$PCs) and dorsomedial striatum (to label $_{ST}$PCs) (**Fig. 1c**). Each PC population resided at characteristic laminar depths, with some overlap: L2 ChCs occupied a similar laminar depth as $_{BLA}$PCs (**Fig. 1c**,**d** and **Supplementary Fig. 3a**). Notably, there was little convergence in projection targets between $_{BLA}$PCs and $_{CC}$PCs (**Fig. 1e**).

To investigate synaptic connectivity between ChCs and $_{BLA}$PCs or $_{CC}$PCs, we performed paired whole-cell patch recordings in L2/3 of PL in which ChCs expressed RFP and either $_{BLA}$PCs or $_{CC}$PCs were retrogradely labeled with CTB-488 (**Fig. 1f**,**g** and **Supplementary Figs. 3b** and **4**). Strikingly, although $_{BLA}$PCs and $_{CC}$PCs had very similar morphological and intrinsic physiological features (**Supplementary Fig. 5**)[20], L2 ChCs preferentially innervated $_{BLA}$PCs over $_{CC}$PCs, indicated by both connection probability (87% vs. 17.5%, 20 of 23 pairs vs. 7 of 40 pairs; $P < 0.01$, Fisher exact test) and synaptic strength measured as the amplitude of unitary postsynaptic current evoked by single action potentials in presynaptic ChCs (ChC→$_{BLA}$PCs: 36.0 ± 4.0 pA, $n = 14$; ChC→$_{CC}$PCs: 11.1 ± 3.4 pA, $n = 7$; $P < 0.001$, Mann–Whitney test) (**Fig. 1h**). This highly selective ChC innervation of $_{BLA}$PCs over $_{CC}$PCs was not explained by differences in their laminar location or distance from ChCs (**Supplementary Fig. 6**). Contrasting with the suggestion from a previous study[9], our results demonstrate remarkable selectivity of ChCs for PC subsets distinguished by projection target, though we cannot exclude the possibility that $_{CC}$PCs might be more strongly controlled by another subset of ChCs.

$_{BLA}$PC-selective ChCs preferentially receive inputs from $_{CC}$PCs

To examine local excitatory inputs to L2 ChCs, we recorded synaptic currents in ChCs following spikes evoked in either $_{BLA}$PCs or $_{CC}$PCs

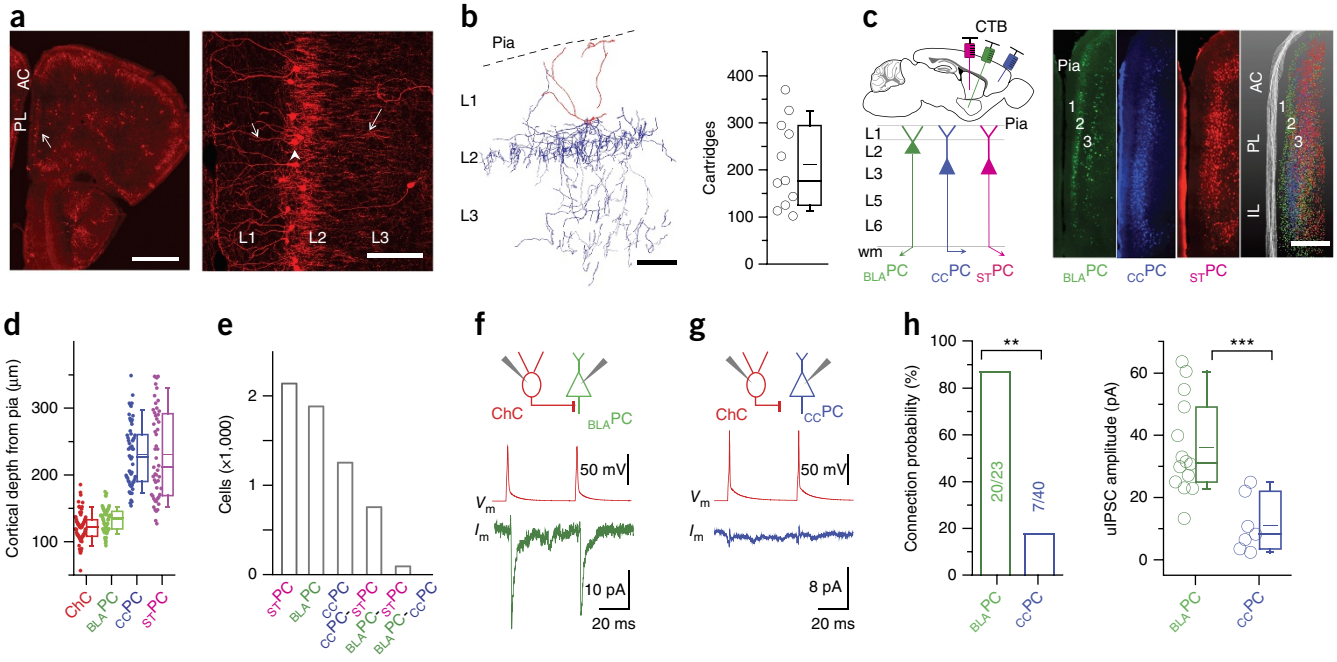

Figure 1 L2 ChCs preferentially innervate $_{BLA}$PCs over $_{CC}$PCs in prelimbic cortex. (**a**) Distribution (left) and morphology (right) of L2 ChCs in PL of an adult *Nkx2.1-CreER:Ai14* mouse tamoxifen-induced at E17.5. Left: arrow indicates PL L2 ChCs. Right: dendrite (short arrow) soma (arrowhead) and axons (long arrow) of ChCs are indicated. Scale bars: 500 μm (left); 100 μm (right). AC: anterior cingulate cortex. (**b**) A Neurolucida reconstruction of a single ChC sparsely labeled in a mouse with low-dose tamoxifen induction (left; scale bar: 50 μm) and counts of total axon cartridges of reconstructed single ChCs ($n = 11$, right). (**c**) Left: a schematic of labeling $_{BLA}$PCs, $_{CC}$PCs and $_{ST}$PCs in PL by injecting three colors of retrograde CTB (Alexa 488, 594, 648) to the three corresponding brain areas in the same mouse. Right: distribution patterns of three PC subsets in medial prefrontal cortex in single sections (100 μm thickness) and in overlay (1 mm thickness). Scale bar: 500 μm; wm, white matter. (**d**) Average cortical depth of ChCs and three types of PCs in upper layers of the PL (cut off at 350 μm from pia) in the example section ($_{BLA}$PC: 133.1 ± 2.3 μm, $n = 63$; $_{CC}$PC: 230.3 ± 6.1 μm, $n = 60$; $_{ST}$PC: 231.3 ± 9.5 μm, $n = 52$; ANOVA, $P < 0.001$). $_{BLA}$PCs are located at similar laminar depth as ChCs (121.9 ± 2.7 μm, $n = 69$) but more superficial to $_{CC}$PCs ($P < 0.001$, Mann–Whitney test). (**e**) Total number of cells that exhibit single or double labeling of CTB, indicating specific or bifurcating axonal projections to injection sites. Of a total 6,163 PCs counted, there were only 43 cells co-staining for BLA and contralateral cortex projections. (**f**,**g**) Examples of synaptic responses from ChC to $_{BLA}$PC and to $_{CC}$PC. Top panels: schematic of dual whole-cell patch recording of a ChC (red) and a $_{BLA}$PC or $_{CC}$PC labeled by CTB. Bottom panels: representative traces from paired recordings in a $_{BLA}$PC (green) or a $_{CC}$PC (blue), showing unitary inhibitory postsynaptic currents (uIPSCs, averaged from 20–30 trials) evoked by paired action potentials in presynaptic ChCs. (**h**) Summaries of ChC-to-PC connection probability (numbers in graph indicate connected/tested pairs; $^{**}P < 0.01$, Fisher exact test) and uIPSC magnitude (each circle represents individual connections; ChC→$_{BLA}$PCs, $n = 14$; ChC→$_{CC}$PCs, $n = 7$; $^{***}P < 0.001$, Mann–Whitney test). Box plots indicate median (full horizontal bar), mean (partial horizontal bar), quartiles and range.

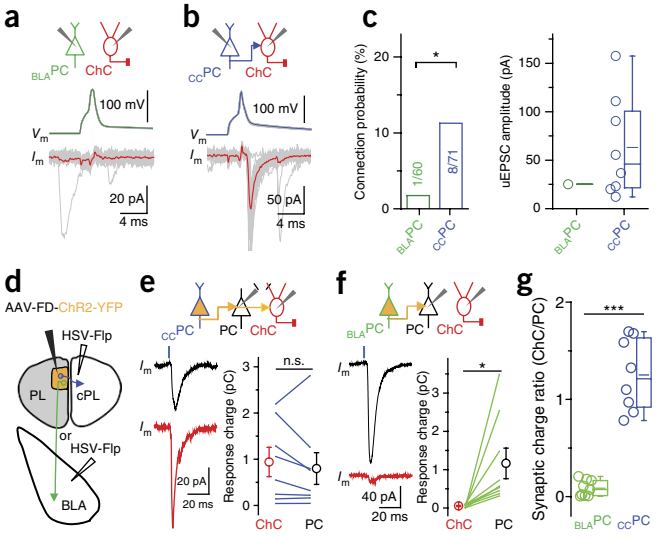

Figure 2 L2 ChCs receive strong input from $_{CC}$PCs and weak input from $_{BLA}$PCs. (**a**,**b**) Examples of synaptic responses in ChCs (red) following action potentials evoked in a $_{BLA}$PC (**a**, green) and a $_{CC}$PC (**b**, blue). Top: schematic of dual recordings. Bottom: representative traces from paired recordings in ChCs, averaged with thick traces from 20–30 trials. (**c**) Summaries of PC-to-ChC connection probability (numbers in bar graph indicate connected/tested pairs; $^*P = 0.038$, Fisher exact test) and unitary excitatory postsynaptic current (uEPSC) magnitude, including results from experiments using loose patch of presynaptic PCs (see **Supplementary Fig. 6**). (**d**) Schematic of dual viral delivery with retrograde HSV-Flp injection at cPL (top) or ipsilateral BLA (bottom), followed by AAV-FD-ChR2-YFP injection in PL. (**e**) Top: optical stimulation of $_{CC}$PCs (blue) and whole-cell recording of postsynaptic responses in an adjacent PC (black) and ChC (red) pair. Bottom left: example monosynaptic responses from a PC (black) and a nearby ChC (red) evoked by optical stimulation, indicated by the blue bar, averaged from 10 trials. Bottom right: summary of synaptic response charges of paired neurons, indicated by lines, in $_{CC}$PCs expressing ChR2 ($n = 8$ pairs, $P = 0.35$, $t = 0.99$, Student's paired t-test); average values indicated by circles (data are presented as mean ± s.e.m.; n.s., not significant). (**f**) The same configuration as in **e** with optical stimulation of $_{BLA}$PCs (green) ($n = 9$ pairs, $^*P = 0.02$, $t = -2.91$, Student's paired t-test). (**g**) Comparison of the ratio of synaptic response charge of ChCs over adjacent PCs following optical stimulation of the ChR2 axon from $_{BLA}$PCs ($n = 9$) and $_{CC}$PCs ($n = 8$, $^{***}P < 0.001$, Mann–Whitney test). Box plots indicate median (full horizontal bar), mean (partial horizontal bar), quartiles and range.

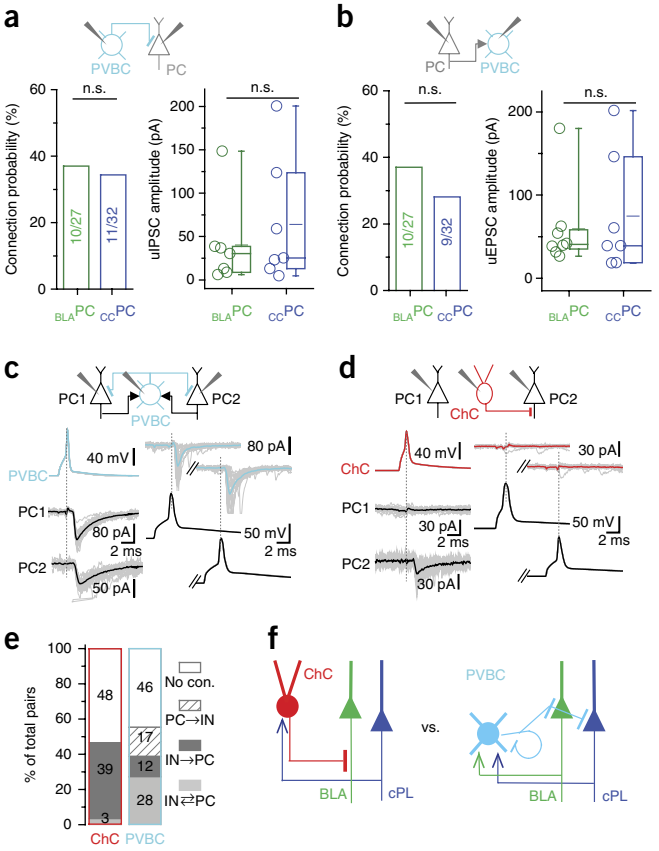

Figure 3 Distinct local circuit connectivity of PVBCs and ChCs in PL upper layers. (**a**,**b**) Summaries of PVBC-to-PC (**a**) and PC-to-PVBC (**b**) connection probability (numbers in graph indicate connected/tested pairs. PVBC→PC: $\chi^2 = 1.04$, $P = 0.31$; PC→PVBC: $\chi^2 = 1.84$, $P = 0.17$; Pearson chi-squared test) and of the strength of uIPSC and uEPSC (each circle representing individual connections; PVBC→$_{BLA}$PCs, $n = 9$; PVBC→$_{CC}$PCs, $n = 7$; $P = 0.46$. $_{BLA}$PC→PVBCs, $n = 8$; $_{CC}$PC→PVBC, $n = 7$; $P = 0.95$; Mann–Whitney test). Top: schematic of dual whole-cell patch recording of a PVBC (cyan) and a PC (gray, $_{BLA}$PC or $_{CC}$PC) labeled by CTB. Plots indicate median (full horizontal bar), mean (partial horizontal bar), quartiles and range; n.s., not significant. (**c**) Triple recording scheme and an example showing reciprocal connectivity in the PVBC microcircuit, with IPSC traces in both PCs evoked by PVBC spikes and EPSC traces in the PVBC evoked by spikes in either PC, averaged in thick trace from 15–20 trials. (**d**) Similar configuration as in **c** with ChC instead of PVBC. (**e**) Summary of connectivity patterns in ChC or PVBC microcircuits in PL upper layer. Numbers in the bar graph indicate the number of pairs in each connection category. (**f**) Schematic of two distinct microcircuit modules mediated by ChC and PVBC, respectively.

(**Fig. 2a**,**b** and **Supplementary Fig. 7**). Whereas 11.3% of $_{CC}$PCs innervated ChCs (8 in 71 pairs, synaptic strength = 63.2 ± 18.3 pA), only 1 $_{BLA}$PC→ChC connection was observed in 60 tested pairs ($P < 0.05$, Fisher exact test) (**Fig. 2c**). This selective input from $_{CC}$PCs over $_{BLA}$PCs was even more striking considering that $_{BLA}$PCs were located closer to ChCs than $_{CC}$PCs (**Fig. 1d**).

To assay inputs from broader populations of $_{CC}$PCs and $_{BLA}$PCs, we expressed channelrhodopsin-2 (ChR2) in each subset using a dual viral delivery strategy. A Flp-expressing retrograde herpes simplex virus (HSV-Flp) was first injected to either contralateral PL (cPL) or ipsilateral BLA; this was followed by the injection of a Flp-dependent ChR2-expressing adeno-associated virus (AAV-FD-ChR2-YFP) in PL to express ChR2 in $_{CC}$PCs or $_{BLA}$PCs, respectively (**Fig. 2d** and **Supplementary Fig. 8**; also see Online Methods). We then performed paired recordings of L2 ChCs and adjacent ChR2$^-$ PCs to measure the monosynaptic input from ChR2$^+$ PCs (see Online Methods). Optical stimulation of ChR2$^+$$_{CC}$PC axons evoked prominent monosynaptic responses in ChCs that were of similar strength to those in adjacent PCs ($n = 8$ pairs; ChCs: 0.94 ± 0.32 pC; PCs: 0.80 ± 0.34 pC; $P = 0.35$, Student's paired t-test) (**Fig. 2e**). However, stimulation of $_{BLA}$PCs evoked extremely weak synaptic responses in ChCs ($n = 9$ pairs; ChCs: 0.05 ± 0.01 pC; PCs: 1.16 ± 0.40 pC; $P = 0.02$, Student's paired t-test) (**Fig. 2f**). We evaluated the strength of these inputs using the ratio of synaptic response charge in ChC vs. PC for each pair ($_{CC}$PC local input: 1.25 ± 0.14; $_{BLA}$PC local input: 0.09 ± 0.03; $P < 0.001$, Mann–Whitney test) (**Fig. 2g**). Thus, L2 ChCs receive much stronger input from $_{CC}$PCs than from $_{BLA}$PCs, a recruitment specificity exactly opposite to their innervation specificity.

ChCs and PVBCs form distinct microcircuit modules

As a comparison, we also assayed the connectivity pattern of PVBCs, which innervate the perisomatic region of PCs and also control PC

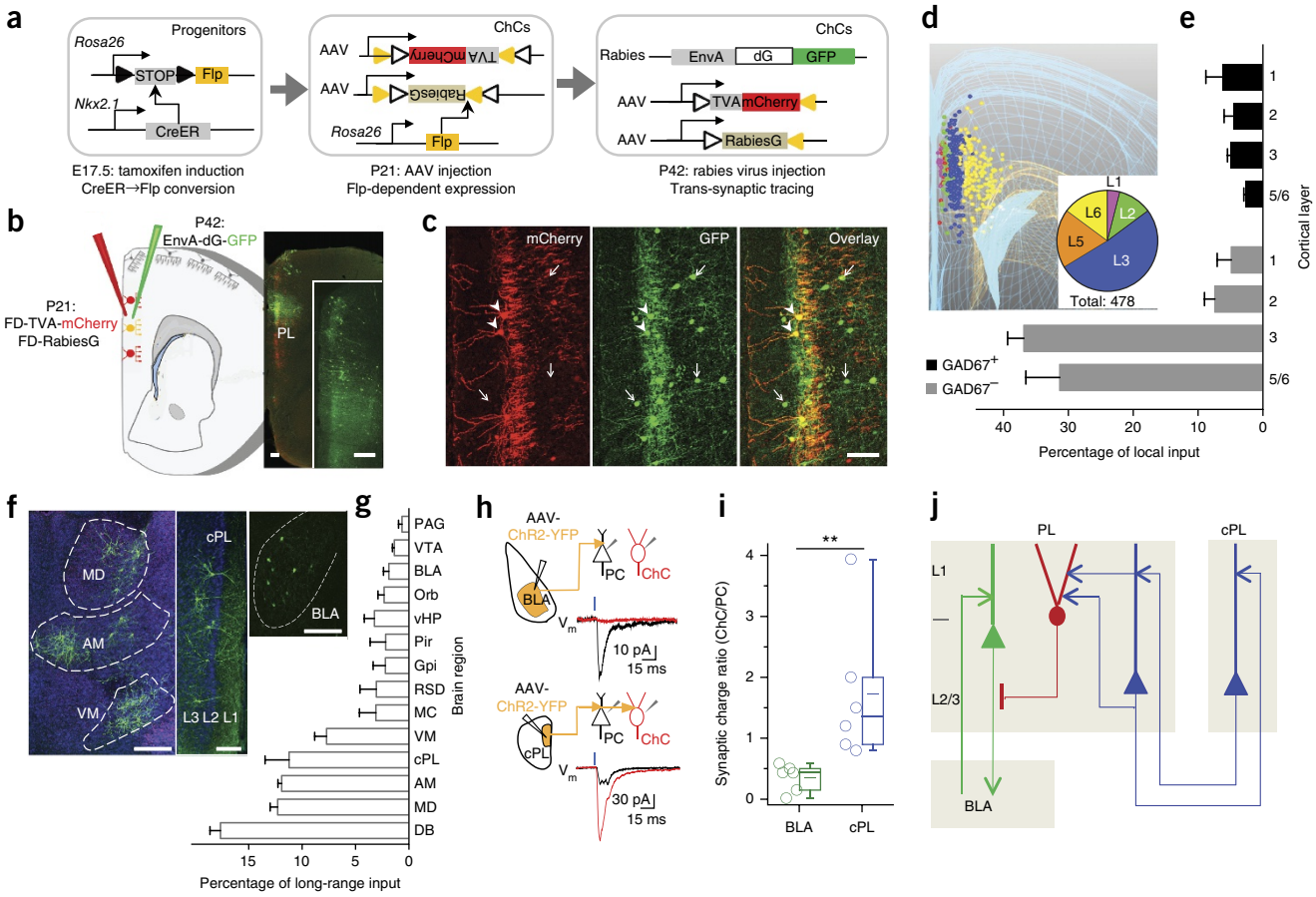

Figure 4 Systematic tracing of local and long-range inputs reveal that L2 ChCs are preferentially recruited by bilateral $_{CC}$PC input as opposed to BLA input. (**a**) Scheme for converting transient CreER activity in Nkx2.1^{+} progenitors to permanent Flp activity in ChCs, which enables AAV and rabies viral targeting in mature cortex. (**b**) Left: schematic of trans-synaptic rabies tracing specifically from PL L2 ChCs. Right: overview of PL region triple-infected with AAV-FD-TVA-mCherry, AAV-FD-RabiesG, and rabies-EnvA-dG-GFP. Inset: overview of PL region with GFP expression. Scale bar: 200 µm. (**c**) Example of retrograde trans-synaptic tracing from L2 ChCs in PL. Triple-infected ChC starter cells coexpress mCherry and GFP (arrowheads); some of their pre-synaptic cells incorporated GFP through rabies-GFP (arrows). Scale bar: 100 µm. (**d**) A 3D stereological rendering and reconstruction of total local inputs to PL L2 ChCs from a single tracing experiment. The laminar distributions of presynaptic cells are colored and their ratios presented as a pie chart. (**e**) Laminar source of local input to L2 ChCs separated by GABAergic or glutamatergic cells (n = 5 mice; see **Supplementary Fig. 8**). Data are presented as mean + s.e.m. (**f**) Examples of long-range input sources to PL L2 ChCs, indicated by GFP labeling in several thalamic nuclei, cPL and BLA. Scale bars: 100 µm. (**g**) Distribution of long-range inputs to PL L2 ChCs (n = 5 mice) measured as percentage of the total number of presynaptic cells detected brain wide. Data are presented as mean + s.e.m. (PAG: periaqueductal gray; VTA: ventral tegmental area; Orb: orbitofrontal cortex; vHP: ventral hippocampus; Pir: piriform area; Gpi: globus pallidus internal segment; RSD: retrosplenial area dorsal part; MC: motor cortex; VM, AM, MD: mediodorsal, anteromedial, ventromedial thalamic nuclei; DB: diagonal band). (**h**) Examples of synaptic responses in pairs of adjacent ChCs (red) and PCs (black) evoked by optical stimulation (the blue bar) of ChR2-expressing BLA (top) or cPL (bottom) input axons. Left schematics depict stimulation and recording configurations after AAV-ChR2 infection of BLA or cPL. Synaptic responses were averaged from 10 trials. (**i**) Summary of the ratio of synaptic response charge of ChCs over adjacent PCs following optical stimulation of the ChR2 axon from BLA (n = 6) or cPL (n = 6; $^{**}P < 0.01$, Mann–Whitney test). Plots indicate median (full horizontal bar), mean (partial horizontal bar), quartiles and range. (**j**) Schematic model: L2 ChCs in the PL mediate directional inhibition in local circuits from $_{CC}$PCs to $_{BLA}$PCs and in global networks from the bilateral $_{CC}$PC reciprocal network to the PL–BLA reciprocal network.

output[22]. Using the *PV-Cre;Ai14* mice, we performed recordings in PL PVBCs and nearby CTB-labeled $_{CC}$PCs or $_{BLA}$PCs. L2/3 PVBCs innervated $_{BLA}$PC and $_{CC}$PC equally in both connection probability (37% vs. 34%, 10 of 27 pairs vs. 11 of 32 pairs; Pearson chi-squared test: $\chi^2 = 1.04$, $P = 0.31$) and synaptic strength (PVBC→$_{BLA}$PCs: 34.5 ± 15.7 pA, n = 9; PVBC→$_{CC}$PCs: 57.0 ± 16.4 pA, n = 7; P = 0.46, Mann–Whitney test) (**Fig. 3a**). In the reverse direction, L2/3 PVBCs received equal inputs from $_{BLA}$PC and $_{CC}$PC in regards to both connection probability (37% vs. 28%, 10 of 27 pairs vs. 9 of 32 pairs; Pearson chi-squared test: $\chi^2 = 1.84$, $P = 0.17$) and synaptic strength ($_{BLA}$PC→PVBCs: 59.4 ± 19.0 pA, n = 8; $_{CC}$PC→PVBC: 74.9 ± 29.0 pA, n = 7; P = 0.95, Mann–Whitney test) (**Fig. 3b**). Thus, in contrast to PL ChCs (and hippocampal PVBCs[23]), PL PVBCs did not selectively connect with projection-defined PC subsets.

To extend this comparison beyond connections with $_{BLA}$PCs and $_{CC}$PCs, we assayed ChC and PVBC connectivity with randomly selected PCs in PL upper layers (**Fig. 3c–e**). PVBCs formed extensive reciprocal connections with adjacent PCs (27.2%, 28 of 103 pairs), consistent with findings in other cortical areas[24,25]. In contrast, ChCs, while extensively innervating nearby PCs (synaptic kinetics shown in **Supplementary Table 1**), formed few reciprocal connections with these synaptic targets (3.3%, 3 of 90 pairs; $P < 0.001$, Fisher exact test). This suggests a unidirectional connectivity pattern consistent with their sending output to $_{BLA}$PCs and receiving input from $_{CC}$PCs.

Therefore, although they both control PC output, ChCs and PVBCs form distinct inhibitory microcircuit modules (**Fig. 3f**).

$_{BLA}$PC-selective ChCs are preferentially recruited by the bilateral PL network

To systematically identify the local and long-range sources of input to L2 ChCs, we designed a genetic strategy that allowed trans-synaptic rabies tracing specifically from ChCs. To enable viral manipulation of ChCs, we generated a *Rosa26-loxpSTOPloxp-Flp* (*LSL-Flp*) mouse line that allowed conversion of transient *Nkx2.1*-driven CreER expression in progenitors of the medial ganglionic eminence to constitutive Flp recombinase expression in ChCs (**Fig. 4a**)[26]. A modified trans-synaptic tracing strategy involving two AAV helpers and a glycoprotein-deleted (dG) rabies virus was used to reveal the overall pattern of local and long-range monosynaptic inputs to L2 ChCs in PL (**Fig. 4b** and Online Methods). We used GAD67 immunostaining to distinguish GABAergic from glutamatergic (GAD67$^-$) neurons labeled by EnvA-dG-GFP. Within the cortex, presynaptic GABAergic neurons (including those positive for PV and vasoactive intestinal peptide) were distributed across cortical layers with slight enrichment in L1 (GAD67$^+$: L1, 5.9 ± 1.4% of total local inputs; L2, 4.5 ± 0.8%; L3, 4.6 ± 0.3%; L5/6, 1.9 ± 0.5%; **Fig. 4c–e** and **Supplementary Fig. 9**). By contrast, presynaptic glutamatergic neurons (GAD67$^-$: L1, 4.7 ± 1.2% of total local inputs; L2, 8.2 ± 1.1%; L3, 40.6 ± 4.6%; L5/6, 30.7 ± 4.2%) were sparse in L2 but were more enriched in L3 and L5/6 (**Fig. 4d,e**), suggesting that L2 ChCs received fewer excitatory inputs from adjacent PCs in the same layer than from PCs in more distant layers, consistent with the paired recording results (**Figs. 1** and **2**).

Major sources of long-range input to L2 ChCs (**Fig. 4f,g**) included the diagonal band of the basal forebrain (16.3 ± 0.9%, including cholinergic input; **Supplementary Fig. 10**); the mediodorsal (11.7 ± 0.7%), anteromedial (11.3 ± 0.3%) and ventromedial (7.3 ± 1.0%) thalamic nuclei; and contralateral PL (cPL; 10.6 ± 2.1%). Although the BLA prominently projects to PL as part of a PL–BLA reciprocal network[20], it was a relatively minor source of long-range inputs to L2 ChCs in the PL (BLA input: 1.8 ± 0.5%). To validate the physiological connections and possible selectivity of long-range inputs, we employed optogenetic measurements to compare the synaptic strength of synapses from cPL and BLA on L2 ChCs. Following AAV-ChR2-YFP injection into BLA or cPL in mice in which ChCs expressed RFP, we performed paired recordings of L2 ChCs and adjacent PCs in the PL upon light activation of ChR2$^+$ BLA or cPL axons, respectively (**Fig. 4h**). We evaluated the strength of these inputs using the ratio of synaptic response charge in ChC vs. PC for each pair. Whereas cPL provided strong input to ChCs (1.72 ± 0.52, n = 6 pairs), BLA sent weak input (0.35 ± 0.10, n = 6 pairs; P < 0.01, Mann–Whitney test) (**Fig. 4i**). Therefore, L2 ChCs in PL not only receive stronger input from local $_{CC}$PCs than from $_{BLA}$PCs, but also receive stronger input from $_{CC}$PCs in cPL than from projection neurons in the BLA. Conversely, BLA neurons project stronger input to $_{BLA}$PCs than $_{CC}$PCs in the superficial layers, and contralateral $_{CC}$PCs provide similar input to $_{BLA}$PCs and $_{CC}$PCs[20]. Taken together, these data suggest that the ChCs are preferentially recruited by the reciprocal network comprising callosally projecting $_{CC}$PCs from the two hemispheres (PL–cPL network), compared to the reciprocal PL–BLA network (**Fig. 4j**).

L2 ChCs suppress PC firing in freely behaving mice

To examine the physiological impact of ChCs on PCs *in vivo*, we combined optogenetic manipulation of ChCs with single-unit recording of PCs in freely behaving mice. We virally expressed ChR2 in L2 ChCs by injecting AAV-FD-ChR2-YFP into the PL of mice expressing *Flp*

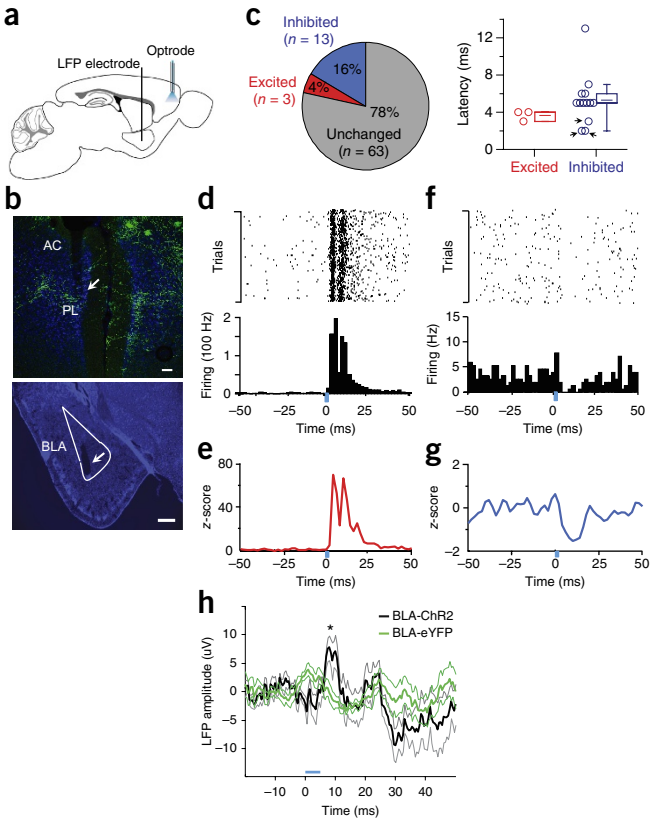

Figure 5 Optogenetic activation of L2 ChCs in PL inhibits PL firing, including $_{BLA}$PC firing, in freely behaving mice. (**a**) Schematic of optrode stimulation and recording in the upper layer of PL with simultaneous LFP monitoring in ipsilateral BLA. (**b**) A coronal section from a *Nkx2.1-CreER;LSL-Flp* mouse brain with bilateral infection by AAV-FD-ChR2-YFP in the PL. Arrows indicate the optrode track through the frontal cortex (top) and the electrolytic lesion from the LFP electrode in the BLA (bottom). Green, ChR2; blue, DAPI; scale bars, 100 µm; AC, anterior cingulate. (**c**) Percentages (left) and latencies (right) of statistically significant excited or inhibited PL single units. Significance determined by bootstrapping (see Online Methods). Note the three inhibited units with very short latency (≤3 ms; arrows). Plots indicate median (horizontal bar), quartiles and range. (**d**) Spike raster (top) and peri-stimulus time histogram (PSTH, bottom) for a light-excited unit that increased firing within 15 ms of light onset (blue bar). Light pulse duration, 5 ms; frequency, 1 Hz. (**e**) Average PSTH for the three short-latency light-excited units. (**f**,**g**) Same as in **d**,**e** for short-latency light-inhibited units. (**h**) Evoked potential in BLA during the optical stimulation of PL. Blue bar indicates light pulse. Average evoked potential 5–10 ms following light pulse was significantly different between control and the ChR2 group (ChR2: 5.58 ± 3.56 µV, n = 6 sessions from 3 mice; eYFP: –0.38 ± 3.57 µV, n = 5 sessions from 3 mice; $^*P$ < 0.05, t = 2.41, two-sample t-test).

in ChCs (**Fig. 4a**). Of total virally labeled cells, 88.6 ± 5.6% cells were ChCs; in layer 2/3 specifically, 94.8 ± 3.6% of cells were ChCs (n = 5 mice; **Supplementary Fig. 11**). We implanted optrodes targeting the PL and field electrodes targeting the ipsilateral BLA (**Fig. 5a,b**; also see Online Methods). In the PL, 79 well-isolated single units were recorded in freely moving mice (n = 3) in a small, dark box. Following brief (5 ms, 5 mW) pulses of blue light delivered at 1 Hz, 3 of the 79 units showed robust short-latency (3–4 ms) excitatory responses (**Fig. 5c–e**), suggesting that they were likely to be ChR2-expressing ChCs directly activated by light. A larger number of units (13 of 79, 16.5%) were inhibited, typically at longer latencies (ranging from 2 to 13 ms) (**Fig. 5c,f,g**), suggesting that these neurons received monosynaptic

inhibition from ChR2-expressing ChCs. Trial-by-trial analyses showed that such inhibition was independent of the baseline firing state of the unit (**Supplementary Fig. 12**). Notably, three of these inhibited units had latencies (2–3 ms) even shorter than those seen in the three putative ChCs. These short-latency inhibitory responses may have resulted from direct activation of ChC boutons along the AIS of these units, consistent with a fast and powerful inhibition at the spike initiation site. No significant short-latency firing rate responses to light were observed (see Online Methods, "Firing rate analysis") in 65 neurons recorded from control animals (n = 3 mice) expressing eYFP in ChCs.

To assess whether PCs suppressed by ChCs included $_{BLA}$PCs, we first examined the impact of ChC activation on BLA local field potential (LFPs). Our analysis revealed a fast and robust stimulation-evoked positive-going (inhibitory) evoked response in the BLA LFP 5–10 ms following light stimulation in PL (**Fig. 5h**), suggesting that ChC activation suppressed the activity of the PL projection to the BLA. Next, we examined the recordings for evidence of connectivity between the recorded PL single units and the BLA by examining the phase-locking of PL single-unit spikes to BLA 3–6 Hz LFP oscillations[27,28]. Overall, 13 of 79 (16.5%) PL units were significantly phase-locked to the BLA LFP ($P < 0.05$, Rayleigh's test of circular uniformity; see Online Methods). Importantly, the fraction of light-inhibited units that was phase-locked to the BLA LFP (4 of 13, or 31%) was significantly higher than that of units that did not change firing upon ChC activation (9 of 63, or 14%; $P < 0.05$, $\chi^2 = 4.84$, Pearson two-sample chi-squared test) (**Supplementary Fig. 13a**,**b**). Light-inhibited units (8 of 13, or 62%) were also more likely than other units (29 of 58, or 50%) to be more strongly phase-locked to the BLA LFP of the future, suggesting a net PL-to-BLA directionality specifically in the inhibited units (**Supplementary Fig. 13c**,**d**)[29]. Together, these results corroborate those of the *in vitro* experiments, suggesting that ChCs preferentially inhibit $_{BLA}$PCs *in vivo*.

DISCUSSION

A fundamental question in understanding the functional organization of cortical circuits is whether diverse GABAergic neurons mediate more or less the same nonselective, 'blanket' inhibition or contribute to specialized connectivity motifs that shape PC subnetworks underlying specific forms of circuit operations and information processing[4,30,31]. One set of studies suggested a general lack of target selection for neocortical interneurons[32,33], but these studies mostly did not distinguish bona fide interneuron types nor PC subsets. Although certain interneurons may indeed mediate nonselective inhibition in certain circuit contexts—for example, neurogliaform cells[34,35]—several studies have reported selectivity of GABAergic neurons for PC subpopulations in cortex and hippocampus[23,36–38]. In particular, despite the striking subcellular selectivity of ChC innervation[6,7,9], their circuit connectivity pattern is poorly understood[9,11]. Here, by capturing a subset of a bona fide interneuron type and projection-defined PCs, we demonstrate exquisite specificity in the directional innervation as well as recruitment of ChCs not only in local circuits but also in global networks. This directional ChC module may promote physiological segregation of intermingled $_{CC}$PC and $_{BLA}$PC ensembles. As $_{CC}$PC and $_{BLA}$PC are each embedded in distinct larger scale networks, this might provide a cellular basis for hierarchical control of one brain network (the PL–cPL network) over another (PL–BLA network). These results suggest that the specialization of interneuron subpopulations in the inhibitory control of discrete PC ensembles might be a key principle of cortical organization. These ensembles might then be combined to construct hierarchical or parallel information processing streams in global networks. Defining the features and degrees of inherent specificity of such connectivity templates will thus provide biological ground truth for building models of cortical computation and information processing.

A key prerequisite to discovering the specificity of neural connectivity is the identification of appropriate neuronal subpopulations or subtypes—basic building blocks of circuit motifs and network scaffolds[39]. While several major classes or populations of cortical GABAergic neurons have been recognized, the specific subpopulations that constitute functional circuit modules remain largely unknown. In the hippocampus, a recent set of studies demonstrated that PVBCs consist of subpopulations with distinct embryonic birth date, input connectivity and output target neurons, each subpopulation playing distinct roles in network level plasticity and learning[40,41]. In this context, it should be noted that cortical ChCs are generated from Nkx2.1-positive progenitors during late gestation[21], mainly between E15.5 and E18.5, and our current results on their wiring specificity are derived from a subset of L2 ChCs born at E17.5 or later. It is possible that earlier-born ChCs might exhibit different selectivity for PCs, such as $_{CC}$PCs and/or other PC subsets in PL. As E15.5 Nkx2.1-positive progenitors generate a large proportion of non-ChCs, a more refined genetic tool that targets earlier-born ChCs will facilitate examining this intriguing possibility.

The extensive control of PC firing by PV- and cholecystokinin (CCK)-positive basket interneurons, both innervating the perisomatic region[42], raised intriguing questions about the role of ChCs that target the AIS. Here we demonstrate that, beyond their differences in subcellular selectivity, ChCs and PVBCs differ substantially in their local connectivity and therefore represent distinct microcircuit modules. While PVBC–PC connectivity is extensively reciprocal and largely nonselective, connectivity between ChCs and PCs is directional and highly selective. While the multipolar dendrites of L2/3 PVBCs receive dense inputs from local PCs, the predominant apical layer 1 dendrites of ChCs receive sparse local excitatory inputs but more extensive inputs from other cortical layers and diverse long-range sources. ChCs and PVBCs further differ in their *in vivo* spike timing during brain state transitions and coupling to network oscillations[43]. Together, these results suggest that PVBCs are well suited to regulating the balance, gain and network oscillation of relatively broad PC populations[22,42]. ChCs may instead mediate the dynamic segregation and hierarchical interaction of select PC ensembles, thereby routing information flow through local circuits and global networks, especially in response to more distant and long-range inputs.

We provide, to our knowledge, the first compelling evidence that ChCs inhibit PC firing *in vivo*. However, we studied a restricted subset of ChCs in PL L2. It is possible that the physiological impact of the other ChCs varies in different layers, brain areas. Our results do not exclude the possibility that ChCs might also exert excitatory effects under certain network states (for example, the down state) when the PC AIS is substantially more hyperpolarized from the chloride equilibrium potential[14]. Future studies that monitor and manipulate ChCs in behavioral tasks that engage different brain states will further clarify the cellular influence of ChCs in orchestrating dynamic PC ensembles and circuit operations[44]. Because of the low and variable efficiency of ChC targeting by tamoxifen induction and virus infection, the exact role of PL units inhibited by these ChCs remains to be further examined.

In associative fear learning, the activity of PVBCs in PL is modulated by conditioned stimuli and contributes to the synchronization of PC firing (including $_{BLA}$PC) that drives fear expression[45,46]. Given their selective and directional inhibition of $_{BLA}$PC and likely the PL–BLA network, ChCs, in contrast to PVBCs, may suppress fear expression according to upstream signals. In this context, our finding that ChCs receive major inputs from the bilateral $_{CC}$PC network and the

mediodorsal thalamus (MD) is noteworthy. As a high-order thalamic nucleus, MD integrates inputs from orbitofrontal cortex, medial frontal cortex, BLA and basal ganglia, projects to prefrontal cortex[17,18,47], and has been implicated in working memory and cognitive flexibility[48]. It is thus possible that an inhibitory control of the $_{BLA}$PC-BLA network by the MD–$_{CC}$PC network through L2 ChCs might contribute to cognitive and flexible regulation of fear expression.

METHODS

Methods, including statements of data availability and any associated accession codes and references, are available in the online version of the paper.

Note: Any Supplementary Information and Source Data files are available in the online version of the paper.

ACKNOWLEDGMENTS

We thank S. Schamiloglu for help with retrograde labeling of PL pyramidal neurons, B. Li, A. Kepecs and G. Buzsáki for comments on the manuscript. This work was supported in part by NIH R01 MH094705-05 and CSHL Robertson Neuroscience Fund to Z.J.H. and by NIH R01 MH081968 and the Hope for Depression Research Foundation to J.A.G. J.T. was supported by NRSA F30 Medical Scientist Predoctoral Fellowships. J.L. was supported by a NARSAD Postdoctoral Fellowship. N.P.C. was supported by the National Science Foundation. J.A.G. contributed to this article while at Columbia University, before joining the National Institute of Mental Health. The views expressed are the author's own and do not represent the views of the National Institutes of Health, the Department of Health and Human Services, or the United States government.

AUTHOR CONTRIBUTIONS

J.L. carried out electrophysiological and optogenetic studies of synaptic connectivity; J.T. performed anatomical and rabies synaptic tracing studies and contributed to in vivo and in vitro physiology studies and analyses; N.P.-C. performed in vivo electrophysiological recordings and data analysis; J.A.G. supervised in vivo electrophysiological recordings and data analysis; M.H. generated the LSL-Flp mouse line; Z.J.H. conceived and organized the study, and wrote the manuscript with contributions from all authors.

COMPETING FINANCIAL INTERESTS

The authors declare no competing financial interests.

1. Harris, K.D. & Shepherd, G.M. The neocortical circuit: themes and variations. *Nat. Neurosci.* **18**, 170–181 (2015).
2. Somogyi, P., Katona, L., Klausberger, T., Lasztóczi, B. & Viney, T.J. Temporal redistribution of inhibition over neuronal subcellular domains underlies state-dependent rhythmic change of excitability in the hippocampus. *Phil. Trans. R. Soc. Lond. B* **369**, 20120518 (2013).
3. Huang, Z.J. Toward a genetic dissection of cortical circuits in the mouse. *Neuron* **83**, 1284–1302 (2014).
4. Roux, L. & Buzsáki, G. Tasks for inhibitory interneurons in intact brain circuits. *Neuropharmacology* **88**, 10–23 (2015).
5. Somogyi, P. A specific 'axo-axonal' interneuron in the visual cortex of the rat. *Brain Res.* **136**, 345–350 (1977).
6. DeFelipe, J., Hendry, S.H., Jones, E.G. & Schmechel, D. Variability in the terminations of GABAergic chandelier cell axons on initial segments of pyramidal cell axons in the monkey sensory-motor cortex. *J. Comp. Neurol.* **231**, 364–384 (1985).
7. Somogyi, P. *et al.* Identified axo-axonic cells are immunoreactive for GABA in the hippocampus and visual cortex of the cat. *Brain Res.* **332**, 143–149 (1985).
8. Tamás, G. & Szabadics, J. Summation of unitary IPSPs elicited by identified axo-axonic interneurons. *Cereb. Cortex* **14**, 823–826 (2004).
9. Inan, M. *et al.* Dense and overlapping innervation of pyramidal neurons by chandelier cells. *J. Neurosci.* **33**, 1907–1914 (2013).
10. Crick, F. & Asanuma, C. Certain aspects of the anatomy and physiology of cerebral cortex. in *Parallel Distributed Processing: Exploration in the Microstructures of Cognition. Vol. 2: Psychology and Biological Models* (eds. Rumelhart, D.E. & McClelland, J.L.) 333–371 (MIT Press, 1986).
11. Woodruff, A.R., Anderson, S.A. & Yuste, R. The enigmatic function of chandelier cells. *Front. Neurosci.* **4**, 201 (2010).
12. Glickfeld, L.L., Roberts, J.D., Somogyi, P. & Scanziani, M. Interneurons hyperpolarize pyramidal cells along their entire somatodendritic axis. *Nat. Neurosci.* **12**, 21–23 (2009).
13. Szabadics, J. *et al.* Excitatory effect of GABAergic axo-axonic cells in cortical microcircuits. *Science* **311**, 233–235 (2006).
14. Woodruff, A.R. *et al.* State-dependent function of neocortical chandelier cells. *J. Neurosci.* **31**, 17872–17886 (2011).
15. Gabbott, P.L., Warner, T.A., Jays, P.R., Salway, P. & Busby, S.J. Prefrontal cortex in the rat: projections to subcortical autonomic, motor, and limbic centers. *J. Comp. Neurol.* **492**, 145–177 (2005).
16. Hoover, W.B. & Vertes, R.P. Anatomical analysis of afferent projections to the medial prefrontal cortex in the rat. *Brain Struct. Funct.* **212**, 149–179 (2007).
17. Delevich, K., Tucciarone, J., Huang, Z.J. & Li, B. The mediodorsal thalamus drives feedforward inhibition in the anterior cingulate cortex via parvalbumin interneurons. *J. Neurosci.* **35**, 5743–5753 (2015).
18. Cruikshank, S.J. *et al.* Thalamic control of layer 1 circuits in prefrontal cortex. *J. Neurosci.* **32**, 17813–17823 (2012).
19. Gilmartin, M.R., Balderston, N.L. & Helmstetter, F.J. Prefrontal cortical regulation of fear learning. *Trends Neurosci.* **37**, 455–464 (2014).
20. Little, J.P. & Carter, A.G. Synaptic mechanisms underlying strong reciprocal connectivity between the medial prefrontal cortex and basolateral amygdala. *J. Neurosci.* **33**, 15333–15342 (2013).
21. Taniguchi, H., Lu, J. & Huang, Z.J. The spatial and temporal origin of chandelier cells in mouse neocortex. *Science* **339**, 70–74 (2013).
22. Hu, H., Gan, J. & Jonas, P. Fast-spiking, parvalbumin^{+} GABAergic interneurons: from cellular design to microcircuit function. *Science* **345**, 1255263 (2014).
23. Lee, S.H. *et al.* Parvalbumin-positive basket cells differentiate among hippocampal pyramidal cells. *Neuron* **82**, 1129–1144 (2014).
24. Lu, J., Tucciarone, J., Lin, Y. & Huang, Z.J. Input-specific maturation of synaptic dynamics of parvalbumin interneurons in primary visual cortex. *Proc. Natl. Acad. Sci. USA* **111**, 16895–16900 (2014).
25. Yoshimura, Y. & Callaway, E.M. Fine-scale specificity of cortical networks depends on inhibitory cell type and connectivity. *Nat. Neurosci.* **8**, 1552–1559 (2005).
26. He, M. *et al.* Strategies and tools for combinatorial targeting of GABAergic neurons in mouse cerebral cortex. *Neuron* **91**, 1228–1243 (2016).
27. Karalis, N. *et al.* 4-Hz oscillations synchronize prefrontal-amygdala circuits during fear behavior. *Nat. Neurosci.* **19**, 605–612 (2016).
28. Likhtik, E., Stujenske, J.M., Topiwala, M.A., Harris, A.Z. & Gordon, J.A. Prefrontal entrainment of amygdala activity signals safety in learned fear and innate anxiety. *Nat. Neurosci.* **17**, 106–113 (2014).
29. Siapas, A.G., Lubenov, E.V. & Wilson, M.A. Prefrontal phase locking to hippocampal theta oscillations. *Neuron* **46**, 141–151 (2005).
30. Karnani, M.M., Agetsuma, M. & Yuste, R. A blanket of inhibition: functional inferences from dense inhibitory connectivity. *Curr. Opin. Neurobiol.* **26**, 96–102 (2014).
31. Krook-Magnuson, E., Varga, C., Lee, S.H. & Soltesz, I. New dimensions of interneuronal specialization unmasked by principal cell heterogeneity. *Trends Neurosci.* **35**, 175–184 (2012).
32. Fino, E. & Yuste, R. Dense inhibitory connectivity in neocortex. *Neuron* **69**, 1188–1203 (2011).
33. Packer, A.M. & Yuste, R. Dense, unspecific connectivity of neocortical parvalbumin-positive interneurons: a canonical microcircuit for inhibition? *J. Neurosci.* **31**, 13260–13271 (2011).
34. Jiang, X. *et al.* Principles of connectivity among morphologically defined cell types in adult neocortex. *Science* **350**, aac9462 (2015).
35. Oláh, S. *et al.* Regulation of cortical microcircuits by unitary GABA-mediated volume transmission. *Nature* **461**, 1278–1281 (2009).
36. Lee, A.T. *et al.* Pyramidal neurons in prefrontal cortex receive subtype-specific forms of excitation and inhibition. *Neuron* **81**, 61–68 (2014).
37. Otsuka, T. & Kawaguchi, Y. Cortical inhibitory cell types differentially form intralaminar and interlaminar subnetworks with excitatory neurons. *J. Neurosci.* **29**, 10533–10540 (2009).
38. Varga, C., Lee, S.Y. & Soltesz, I. Target-selective GABAergic control of entorhinal cortex output. *Nat. Neurosci.* **13**, 822–824 (2010).
39. Caroni, P. Inhibitory microcircuit modules in hippocampal learning. *Curr. Opin. Neurobiol.* **35**, 66–73 (2015).
40. Donato, F., Chowdhury, A., Lahr, M. & Caroni, P. Early- and late-born parvalbumin basket cell subpopulations exhibiting distinct regulation and roles in learning. *Neuron* **85**, 770–786 (2015).
41. Donato, F., Rompani, S.B. & Caroni, P. Parvalbumin-expressing basket-cell network plasticity induced by experience regulates adult learning. *Nature* **504**, 272–276 (2013).
42. Armstrong, C. & Soltesz, I. Basket cell dichotomy in microcircuit function. *J. Physiol. (Lond.)* **590**, 683–694 (2012).
43. Massi, L. *et al.* Temporal dynamics of parvalbumin-expressing axo-axonic and basket cells in the rat medial prefrontal cortex in vivo. *J. Neurosci.* **32**, 16496–16502 (2012).
44. Viney, T.J. *et al.* Network state-dependent inhibition of identified hippocampal CA3 axo-axonic cells in vivo. *Nat. Neurosci.* **16**, 1802–1811 (2013).
45. Courtin, J. *et al.* Prefrontal parvalbumin interneurons shape neuronal activity to drive fear expression. *Nature* **505**, 92–96 (2014).
46. Dejean, C. *et al.* Prefrontal neuronal assemblies temporally control fear behaviour. *Nature* **535**, 420–424 (2016).
47. Mátyás, F., Lee, J., Shin, H.S. & Acsády, L. The fear circuit of the mouse forebrain: connections between the mediodorsal thalamus, frontal cortices and basolateral amygdala. *Eur. J. Neurosci.* **39**, 1810–1823 (2014).
48. Parnaudeau, S. *et al.* Inhibition of mediodorsal thalamus disrupts thalamofrontal connectivity and cognition. *Neuron* **77**, 1151–1162 (2013).

ONLINE METHODS

Experimental animals. To genetically label and manipulate chandelier cells, we crossed *Nkx2.1-CreER* mice (The Jackson Laboratory stock 014552) with either *Rosa26-loxpSTOPloxp-TdTomato* (*Ai14*) reporter (The Jackson Laboratory stock 007905) or in-house-derived *Rosa26-loxpSTOPloxp-Flp* (*LSL-Flp*) mice[26]. To properly identify embryonic day 17.5 (E17.5) for tamoxifen (TM) inductions, Swiss Webster females (Taconic) were housed with *Nkx2.1-CreER* (heterozygous);*Ai14* (homozygous) males overnight and females were checked for a vaginal plug by 8–9 a.m. the next morning. Positive plug identification was designated E0.5. To genetically label parvalbumin-positive basket cells (PVBCs), we crossed *PV-Cre* mice (The Jackson Laboratory stock 008069) with *Ai14* reporter mice. The ages of animals used are indicated in the different experiments stated below. Both male and female mice were employed without distinction in all experiments. All experiments were conducted in accordance with the Institutional Animals Care and Use Committee of Cold Spring Harbor Laboratory.

Tamoxifen induction. TM was dissolved in corn oil (20 mg/ml) overnight, at room temperature under constant stirring. Stocks were stored as individual aliquots at 4 °C for no more than 1 month. After light isoflurane anesthesia pregnant females were given oral gavage administration of TM (dose: 3 mg per 30 g of body weight) at gestational day E17.5 for dense labeling of ChCs. In rare instances, TM induction led to dystocia in pregnant females and emergency caesarian sections were performed. Pups retrieved by caesarians were housed with Swiss Webster foster mothers until weaning age. For the experiment involving sparse labeling of ChCs for single cell reconstruction, a low dose of TM (0.1 mg per 30 g of body weight) was used.

Viral constructs. HSV-Elf1a-Flp was purchased from Rachael Neve, Viral Gene Transfer Core, MIT; AAV-Elf1a-FD-ChR2-YFP was a gift from the Deisseroth laboratory, Stanford University. AAV-CAG-ChR2-YFP was purchased from the UNC vector core, Chapel Hill, North Carolina. Ef1a-FD-TVA-mcherry (TVA: avian glycoprotein EnvA receptor) and Ef1a-FD -RabiesG (RabiesG: rabies glycoprotein) cassettes were assembled and cloned using standard molecular cloning protocols with restriction enzymes from New England Biolabs. TVA-mCherry (pAAV-EF1a-FLEX-TVA-mCherry) was a gift from Naoshige Uchida (Addgene plasmid # 38044); RabiesG (pAAV-CA-FLEX-RG) was a gift from Naoshige Uchida (Addgene plasmid # 38043)). Each assembled cassette was subcloned into AAV-Ef1a-FD-YFP-WPRE (a gift from the Deisseroth laboratory, Stanford University)[49] using NheI and AscI cloning sites. All constructs were sequenced to ensure their fidelity and proper reversed orientation of the inserts, and packed into AAV8 viral vectors with titers ranging from 1.0×10^{12} to 2.4×10^{12} pfu from the UNC Vector Core (Chapel Hill, North Carolina). A pseudotyped rabies virus expressing the avian glycoprotein EnvA (EnvA-dG-GFP, 4.3×10^{8} pfu) was purchased from Salk GT3 Vector Core (La Jolla, California).

Surgical procedures for stereotaxic injection. Animals were anesthetized by an intraperitoneal injection of ketamine and xylazine (100 mg/kg ketamine, 10 mg/kg xylazine in saline). Mice were mounted in a stereotaxic headframe (Kopf Instruments model 940 series). Bregma coordinates were identified for four brain areas: PL and contralateral PL (cPL) (antero-posterior, A/P: 2.0 mm; medio-lateral, M/L: 0.2–0.3 mm; dorso-ventral, D/V: 1.5 mm depth from the pial surface), BLA (A/P: −1.6 mm, M/L: 3.0–3.25 mm; D/V: 3.75 mm), dorsomedial striatum (A/P: 1.0 mm; M/L: 1.2 mm; D/V: 2.25). An incision was made over the scalp, a small burr hole was made into the skull and brain surface was exposed. A pulled glass pipette tip of 20–30 µm containing virus or tracers was lowered into the brain. Pulses were delivered using a Picospritzer (General Valve Corp) at a rate of 30 nl/min; the pipette was left in the brain for 5–10 min to prevent backflow[50]. After the injection, the pipette was withdrawn, the incision was closed with tissue glue, and animals recovered.

Retrograde tracing of PC subtypes. For anatomical characterization of PC subsets in PL region, retrograde neuronal tracing with cholera toxin B subunit (CTB) was used. Three colors of CTB (Alexa Fluor 488, 594 and 647) (Life Technologies, 0.3 µl, 2% in PBS) were injected into BLA, dorsomedial striatum, and cPL in the same mouse, respectively. The laminar distribution and co-staining analysis was performed as described below.

For physiological paired recordings, CTB-488 (0.3 µl, 2% in PBS) was injected into either BLA or cPL to label $_{BLA}$PC or $_{CC}$PC in the PL upper layer. We verified *post hoc* the proper placement of injection site for physiological experiments. For all CTB experiments animals were either perfused or prepared for slice physiology 5–10 days after injection.

Retrograde rabies tracing. *Virus injection.* A modified rabies virus strategy was used involving the AAV helper virus and a glycoprotein-deleted (dG) rabies virus to trace monosynaptic inputs to ChCs (**Fig. 4a**,**b**). In *Nkx2.1-CreER;LSL-Flp* mice (TM induction at E17.5), ChCs express Flp at mature ages. At P21, two AAV viruses, a mixture of FD-TVA-mCherry and FD-RabiesG (1:1, 0.3 µl), were injected unilaterally into PL. Flp-expressing ChCs activated the AAV vectors and expressed TVA and RabiesG. Three weeks after AAV injections, 0.3 µl of EnvA-dG-GFP rabies virus was injected at the same PL coordinates so that only the TVA-containing ChCs were infected. The modified rabies virus encodes GFP instead of its native glycoprotein. Cells infected with rabies virus were labeled with mCherry and GFP, allowing their easy identification. These 'starter cells' also expressed RabiesG from the AAV vector, allowing monosynaptic retrograde spread of dG rabies virus. Presynaptic cells expressing GFP from the rabies virus were easily distinguished from the mCherry-labeled starter cells. Animals recovered for 1 week before perfusion to allow sufficient local and long-range labeling with pseudotyped rabies virus. In some cases, in which unpseudotyped rabies injections were used for retrograde labeling of PC ($_{BLA}$PC or $_{CC}$PC) subtypes, 0.5 µl of dG-GFP rabies virus was injected unilaterally into cPL or BLA.

Histology. Seven days after rabies infection, animals were perfused with 4% PFA in PBS. Brains were removed and postfixed overnight using the same fixative. Coronal brain slices were sectioned at 100 µm thickness using a vibratome. For histological analysis of local microcircuitry using GABAergic markers, and analysis of AIS GABA boutons, slices through either the injection site (in the case of rabies input mapping) or PL (in the case of AIS analysis) were sectioned at 20 µm. Sections were blocked with 10% normal goat serum in 0.5% Triton in PBS and then incubated overnight with combinations of the following primary antibodies diluted in blocking solution: rabbit polyclonal RFP (1:1,000, Rockland, catalog number 600-401-379) or chicken polyclonal GFP (1:1,000, Aves, catalog number GFP-1020) for fluorophore preservation of mCherry starter cells and GFP rabies virus expression, mouse monoclonal parvalbumin (1:1,000 Sigma, catalog number P3088), rabbit polyclonal phospho-IκB (1:300, Cell Signaling, catalog number 9242), rabbit polyclonal VIP (1:250, Immunostar, catalog number 20077), rabbit polyclonal somatostatin-14 (1:500, Peninsula, catalog number T4102), mouse monoclonal GAD67 (1:500, EMD Millipore, catalog number MAB5406), mouse monoclonal VGAT (1:500, Synaptic Systems, catalog number 131011), goat polyclonal ChAT (1:500, EMD Millipore, catalog number AB143) and rabbit polyclonal NeuN (1:1,000, Abcam, catalog number Ab104225).

For immunostaining with GAD67, no detergent was used to see somatic labeling for GABA-positive inputs, but detergent was added in samples in which GAD67 boutons were analyzed at the AIS. Sections were incubated with the appropriate Alexa Fluor dye-conjugated IgG secondary antibodies (1:500, Molecular Probes, catalog number A11039 for goat anti-chicken 488, A21244 for goat anti-rabbit 647, A11012 for goat anti-rabbit 594, A11005 for goat anti-mouse 594, A21235 for goat anti-mouse 647 and A31553 for goat anti-mouse 405). In some instances, for identification of distal brain structures such as inputs from particular nuclei of the thalamus and basal forebrain, sections were incubated with Neurotrace fluorescent Nissl stain in secondary antibody (1:300, Molecular Probes, catalog number N21479). Sections were washed and mounted with Fluoromount-G (Southern Biotech, catalog number 0100-01).

Image acquisition and analysis. *Input tracing.* Images were taken by confocal microscopy (Zeiss LSM 780). All images were processed using Fiji[51]. For local input analysis, serial sections through the PL cortex were acquired. In some instances images were spatial registered using the BUnwarp J Fiji plugin[52]. Individual images with Nissl signal were manually overlaid in Photoshop with representative atlas images (Paxinos and Watson *Mouse Brain in Stereotaxic Coordinates*, 3rd edition). For 3D model reconstructions and visualization, image stacks were uploaded and manually traced with the open-source software FreeD[53]. Layers were assigned on the basis of arbitrary assignment of cortical

doi:10.1038/nn.4624

depths (layer 1, 100 μm; layer 2, 100–200 μm; layer 3, 200–400 μm; layer 5/6, >400 μm depth).

Single ChC reconstruction. For single-cell reconstruction in sparse labeling of ChCs, individual cell morphology was traced using Neurolucida software packages (Microbrightfield). Bouton analysis at the AIS of PCs was done with 63× oil immersion lens at a zoom factor of 2.1 and followed previously described protocols[9,54,55]. Briefly, AIS were identified by rabies-GFP label in an axonal process colocalized with phosphor-IκB that was connected to a pyramidal soma. Inhibitory boutons were defined as 0.5- to 1-μm varicosities within more than one 0.3-μm-thick imaging plane and positioned 1 μm or less from an AIS.

***In vitro* electrophysiology.** *Slice preparation.* We used *Nkx2.1-CreER;Ai14* or *PV-Cre;Ai14* mice to investigate the circuit organization of ChC or PVBC network in the PL. Mice (>P30) were anesthetized with isoflurane before decapitation. The dissected brain was rapidly immersed in ice-cold, oxygenated, artificial cerebrospinal fluid (section ACSF: 110 mM choline chloride, 2.5 mM KCl, 4 mM $MgSO_4$, 1 mM $CaCl_2$, 1.25 mM NaH_2PO_4, 26 mM $NaHCO_3$, 11 mM D-glucose, 10 mM sodium ascorbate, 3.1 sodium pyruvate, pH 7.35, 300 mOsm) for 1 min. Coronal prefrontal cortical slices were sectioned at 300 μm thickness using a vibratome (HM 650 V; Microm) at 1–2 °C and incubated with oxygenated ACSF (working ACSF: 124 mM NaCl, 2.5 mM KCl, 2 mM $MgSO_4$, 2 mM $CaCl_2$, 1.25 mM NaH_2PO_4, 26 mM $NaHCO_3$, 11 mM D-glucose, pH 7.35, 300 mOsm) at 34 °C for 30 min, and then transferred to ACSF at room temperature (25 °C) for >30 min before use. Whole cell patch recordings were directed to the medial part of frontal cortex (including PL), using the morphology of subcortical white matter and corpus callosum as primary landmarks according to the atlas (Paxinos and Watson *Mouse Brain in Stereotaxic Coordinates*, 3rd edition).

Electrophysiological recordings. Patch pipettes were pulled from borosilicate glass capillaries with filament (1.2 mm outer diameter and 0.69 inner diameter; Warner Instruments) with a resistance of 3–6 MΩ. The pipette recording solution consisted of 110 mM potassium gluconate, 30 mM KCl, 10 mM sodium phosphocreatine, 10 mM HEPES, 4 mM ATP·Mg, 0.3 mM GTP, and 0.3 mM EGTA (pH 7.3 adjusted with KOH, 290 mOsm). Dual or triple whole-cell recordings from RFP labeled cells at the L1/2 border and CTB-488 labeled PCs in layer 2/3 were made with Axopatch 700B amplifiers (Molecular Devices, Union City, CA) using an upright microscope (Olympus, Bx51) equipped with infrared differential interference contrast optics (IR-DIC) and fluorescence excitation source. In some experiments, PCs, identified by their triangular somata and thick primary dendrites, were blindly selected within 100 μm of an RFP positive interneuron without retrograde tracer. Both IR-DIC and fluorescence images were captured with a digital camera (Microfire, Optronics, CA). All recordings were performed at 33–34 °C with the chamber perfused with oxygenated working ACSF.

Synaptic connection was detected essentially as in ref. 24. Synaptic responses were evoked by presynaptic action potentials (APs) through soma-injected current square wave pulses (1.5–3 ms, 1–2.8 nA). In some experiments, we evoked APs in PCs by loose patch stimulation. The loose patch was achieved by tight touch (>100 MΩ resistance) to the targeted PCs through the same pipette as for the whole cell patch recordings. The stimulation ranged from 0.1 to 1 V in 200 μs, 0.1 Hz. The intensity used was determined by the persistent spikes after the stimulation because the immediate spike was masked by the artifact produced by the stimulation. Recordings were made with two MultiClamp 700B amplifiers (Molecular Devices). The membrane potential was maintained at −75 mV in voltage clamp mode and zero holding current in current clamp mode, without correction of junction potential. The postsynaptic neurons were held at −75 mV when examining synaptic strength. Under this condition, both EPSCs and IPSCs exhibit inward currents. To assess the unitary synaptic transmission strength for the comparison between different groups, the postsynaptic neuron must have adequate access resistance (10–20 MΩ for PCs and PVBCs, 10–25 MΩ for ChCs) and must be able to be well compensated. Both pre- and postsynaptic neurons must be in a stable state during the recording of synaptic strength. During this measurement (0.1 to 0.2 Hz, 30–60 repetitive trials), sometimes cell condition or access resistance deteriorated and recordings had to be ended. Thus in some cases we were able to confirm the presence of connectivity but were not able to measure their strength. Signals were recorded and filtered at 2 kHz, digitized at 20 kHz (Digidata 1322A, Molecular Devices) and further analyzed using pClamp 10.3 software (Molecular Devices) for intrinsic properties and synaptic features.

Optical stimulation of ChR2-expressing pathways. We employed channelrhodopsin-2 (ChR2)-assisted circuit mapping[24] to examine the local and long-range inputs to ChCs using *Nkx2.1-CreER;Ai14* mice. To investigate the local input specificity, we expressed ChR2 in a subset of PCs in PL by injecting AAV- Ef1a-FD-ChR2-YFP unilaterally into PL and simultaneously HSV-Ef1a-Flp into either cPL or BLA. To investigate the long-range inputs, we expressed ChR2 in BLA or contralateral PL by injecting AAV-CAG-ChR2-YFP into BLA or cPL, respectively.

Four to 8 weeks after the injection, monosynaptic responses initiated from $ChR2^+$ axons were recorded in postsynaptic ChCs and adjacent $ChR2^-$ PCs under whole-cell voltage clamp in fresh brain slice. Monosynaptic responses of these inputs were measured in the presence of 1 μM tetrodotoxin (to block action potential generation) and 1 mM 4-aminopyridine (to enhance depolarization of presynaptic terminals). The laser stimulation (447 nm) was flashed (1–3 ms duration, usually 2 ms) on the slices through a fiber LED. The laser power of the optical stimulation system at the focal plane of the slice was determined with stepwise increase of the power. We employed a power that evoked saturated responses (also see **Supplementary Fig. 8**).

***In vivo* electrophysiology.** *Electrode implantation.* Eight to 10 weeks after delivering AAV-Ef1a-FD-ChR2-YFP or AAV-Ef1a-FD-eYFP into the bilateral PL, six *Nkx2.1-CreER;LSL-Flp* mice (TM induction at E17.5) were implanted under isoflurane anesthesia with a custom-made microdrive that contained electrodes and optical fibers. Stereo-optrodes were implanted in the left PL (A/P: −2.00 mm, M/L: 0.20 mm, D/V: −1.18 mm). Each stereo-optrode comprised a 230-μm optical fiber glued to a bundle of 14 tungsten-wire (13 μm diameter) stereotrodes placed 400–500 μm below the end of the optical fiber. Additionally, a 75-μm-diameter tungsten wire field electrode was implanted in the ipsilateral BLA (A/P: −1.60 mm, M/L: 3.3 mm, D/V −4.4 mm). A reference screw was implanted in the skull over the frontal cortex and a ground screw in the skull over the cerebellum.

In vivo *data acquisition.* Data collection occurred 5–7 d after electrode microdrive implantation. The experiment was performed while the animal sat quiescent in a wooden box (20 × 30 cm) in the darkness. We tracked the position of the animal at a sampling rate of 33 Hz. The laser was triggered once per second for 5 ms. There were no differences in distance traveled the ChR2 animals compared to the control animals. During the experiment there were no visible differences between the ChR2 animals and control animals upon laser stimulation. Blue light was delivered using an LED (465 nm; PlexBright LD-1 Single Channel LED Driver from Plexon). Light pulses were 5 ms long and were delivered at 1 Hz. The light power was 5 mW measured from the tip of the optical fiber patch cord. Electrophysiological data were acquired using a Digital Lynx system (Neuralynx). LFPs were referenced to a screw located in the skull over the frontal cortex near the olfactory bulb, band-pass filtered (1–1,000 Hz), and acquired at 2 kHz. Single-unit recordings were band-pass filtered at 600–6,000 Hz and acquired at 32 kHz; spikes were detected by thresholding and sorted off-line. Initial automated spike sorting was done based on the waveform peak, the energy and the first two principal components, using Klustakwik (Ken Harris, UCL) instantiated in SpikeSort3D (Neuralynx); clusters were subsequently manually confirmed. Isolation distance and L-ratio were computed as described in ref. 56. The median isolation distance for the single-unit clusters was 27, and 99% of the units had an isolation distance higher than 10. The median L-ratio was 0.05, and 79% of the units had an L-ratio lower than 0.5.

Firing rate analysis. We used a bootstrapping analysis to determine the statistical significance of firing rate changes. First, for each cell, firing rate was binned in 5-ms bins for 300 ms around each stimulus. Next, 2,000 artificial 'trials' were created by randomly shuffling from these bins. Distributions of firing rates were calculated for bins spanning 0 to 15 ms (for short-latency effects). Units were considered significantly modulated by the stimulus if the actual firing rates in at least three consecutive bins within either interval were below the 5th or above the 95th percentile of the shuffled distributions. This method produced very stringent ($P < 0.001$) requirements for significance. Baseline firing rate reported in **Supplementary Figure 10** consists of the mean firing during 200 ms before laser onset across all trials.

Phase locking and directionality PL–BLA analyses. For BLA field analyses we analyzed 3–6 Hz oscillations, as this frequency range is prominent in the BLA during behavior and has been shown to engage the PL–BLA pathway[27,28]. A given unit was said to be significantly phase locked if the distribution of the BLA LFP phases where the spikes occurred was not uniform as assessed with Rayleigh's

test for non-uniformity of circular data. Zero phase corresponds to the peak of the signal. Phase locking strength was quantified using pairwise phase consistency (PPC)[57]. Shuffled percent of phase locked cells reported in **Supplementary Figure 13b** were calculated by bootstrapping. Spikes were shuffled randomly 1,000 times, phase locking significance was calculated with Rayleigh's test, and for each iteration the percentage of significantly phase locked cells was calculated. On the figure we report the average percent across 1,000 iterations. To calculate the power envelope and phase of BLA theta, a bandpass filter for 3–6 Hz was applied using a zero-phase-delay FIR filter with Hamming window (filter0, provided by K. Harris and G. Buzsáki, New York University), the phase component was calculated by a Hilbert transform, and a corresponding phase was assigned to each spike. To analyze the directionality of PL phase-locking to BLA theta (3–6 Hz), single units with at least 50 spikes were included because the MRL statistic can be highly variable for small spike numbers. The LFP times were lagged relative to the spike timing from −100 ms to 100 ms, stepping by 5 ms, and the MRL value was determined for each single unit at each lag. The MRL at each lag was normalized by dividing by the mean MRL across all lags. For the BLA evoked potential analysis, the BLA LFP was average across all trials (5 ms light presentations) for each animal and the mean evoked potential for 5–10 ms after light presentation was compared across ChR2- and eYFP-injected mice with a two-sample *t*-test.

Analysis and statistics. No statistical methods were used to predetermine sample sizes, but our sample sizes are similar to those reported in previous publications[23,24]. Data distribution was assumed to be normal but this was not formally tested. Data collection and analysis were not performed blind to the conditions of the experiments. No animals or data points were excluded from the analyses. More information about the experimental design and statistics is given in the **Life Sciences Reporting Summary**. For comparison of two groups of data, Mann–Whitney test and Student's paired *t*-test and two-sample *t*-test were used as indicated in the experiment. To compare the observed distributions, Pearson chi-squared tests (Fisher exact tests if any number of samples was below 5) were used. In cases where statistical differences were assessed between brain regions with rabies-traced input sources, one-way ANOVAs were performed followed by Tukey–Kramer tests for mean comparisons. Data are presented as mean ± s.e.m. if not specifically indicated, and $P < 0.05$ was considered significant. Significance is marked as $*P < 0.05$; $**P < 0.01$ and $***P < 0.001$.

Code availability. Code is provided in the **Supplementary Software**.

Data availability. The data that support the findings of this study are available from the corresponding author upon reasonable request.

49. Fenno, L.E. *et al.* Targeting cells with single vectors using multiple-feature Boolean logic. *Nat. Methods* **11**, 763–772 (2014).
50. Kuhlman, S.J. & Huang, Z.J. High-resolution labeling and functional manipulation of specific neuron types in mouse brain by Cre-activated viral gene expression. *PLoS One* **3**, e2005 (2008).
51. Schindelin, J. *et al.* Fiji: an open-source platform for biological-image analysis. *Nat. Methods* **9**, 676–682 (2012).
52. Arganda-Carreras, I. *et al.* Consistent and elastic registration of histological sections using vector-spline regularization. in *Computer Vision Approaches to Medical Image Analysis* 85–95 (Springer, 2006).
53. Andrey, P. & Maurin, Y. Free-D: an integrated environment for three-dimensional reconstruction from serial sections. *J. Neurosci. Methods* **145**, 233–244 (2005).
54. Tai, Y., Janas, J.A., Wang, C.L. & Van Aelst, L. Regulation of chandelier cell cartridge and bouton development via DOCK7-mediated ErbB4 activation. *Cell Rep.* **6**, 254–263 (2014).
55. Wang, X. & Sun, Q.Q. Characterization of axo-axonic synapses in the piriform cortex of *Mus musculus*. *J. Comp. Neurol.* **520**, 832–847 (2012).
56. Schmitzer-Torbert, N., Jackson, J., Henze, D., Harris, K. & Redish, A.D. Quantitative measures of cluster quality for use in extracellular recordings. *Neuroscience* **131**, 1–11 (2005).
57. Vinck, M., van Wingerden, M., Womelsdorf, T., Fries, P. & Pennartz, C.M. The pairwise phase consistency: a bias-free measure of rhythmic neuronal synchronization. *Neuroimage* **51**, 112–122 (2010).

nature research

Corresponding author(s): Z. Josh Huang

☐ Initial submission ☐ Revised version ☒ Final submission

Life Sciences Reporting Summary

Nature Research wishes to improve the reproducibility of the work that we publish. This form is intended for publication with all accepted life science papers and provides structure for consistency and transparency in reporting. Every life science submission will use this form; some list items might not apply to an individual manuscript, but all fields must be completed for clarity.

For further information on the points included in this form, see Reporting Life Sciences Research. For further information on Nature Research policies, including our data availability policy, see Authors & Referees and the Editorial Policy Checklist.

Experimental design

1. Sample size

Describe how sample size was determined.

No statistical methods were used to pre-determine sample sizes but our sample sizes are similar to those reported in previous publications (Lee et al., 2014; Lu et al., 2014)

2. Data exclusions

Describe any data exclusions.

no data were excluded.

3. Replication

Describe whether the experimental findings were reliably reproduced.

All attempts for the replication were successful.

4. Randomization

Describe how samples/organisms/participants were allocated into experimental groups.

The animals and cell samples themselves were genetically targeted. Within each group, the mouse and cell is randomly selected.

5. Blinding

Describe whether the investigators were blinded to group allocation during data collection and/or analysis.

No blinding experiments because the experiments were simple and observative.

Note: all studies involving animals and/or human research participants must disclose whether blinding and randomization were used.

6. Statistical parameters

For all figures and tables that use statistical methods, confirm that the following items are present in relevant figure legends (or in the Methods section if additional space is needed).

n/a	Confirmed	
☐	☒	The exact sample size (*n*) for each experimental group/condition, given as a discrete number and unit of measurement (animals, litters, cultures, etc.)
☐	☒	A description of how samples were collected, noting whether measurements were taken from distinct samples or whether the same sample was measured repeatedly
☐	☒	A statement indicating how many times each experiment was replicated
☐	☒	The statistical test(s) used and whether they are one- or two-sided (note: only common tests should be described solely by name; more complex techniques should be described in the Methods section)
☒	☐	A description of any assumptions or corrections, such as an adjustment for multiple comparisons
☐	☒	The test results (e.g. *P* values) given as exact values whenever possible and with confidence intervals noted
☐	☒	A clear description of statistics including central tendency (e.g. median, mean) and variation (e.g. standard deviation, interquartile range)
☐	☒	Clearly defined error bars

See the web collection on statistics for biologists for further resources and guidance.

Nature Neuroscience: doi:10.1038/nn.4624

Software

Policy information about availability of computer code

7. Software

Describe the software used to analyze the data in this study.	in vitro data were analyzed in Clampfit 10.8 and OriginPro 8.5; in vivo data were analyzed with custom algorithms in Matlab. Some comparison were performed online website: http://www.socscistatistics.com/tests/Default.aspx

For manuscripts utilizing custom algorithms or software that are central to the paper but not yet described in the published literature, software must be made available to editors and reviewers upon request. We strongly encourage code deposition in a community repository (e.g. GitHub). *Nature Methods* guidance for providing algorithms and software for publication provides further information on this topic.

Materials and reagents

Policy information about availability of materials

8. Materials availability

Indicate whether there are restrictions on availability of unique materials or if these materials are only available for distribution by a for-profit company.	no unique materials were used.

9. Antibodies

Describe the antibodies used and how they were validated for use in the system under study (i.e. assay and species).	rabbit polyclonal RFP (1:1000, Rockland) or chicken polyclonal anti-GFP (1:1000, Aves) for fluorophore preservation of mcherry starter cells and GFP rabies virus expression, mouse monoclonal anti-parvalbumin (1:1000 Sigma), rabbit polyclonal phospho-IkappaB (1:300, Cell Signaling), rabbit polyclonal VIP (1:250, Immunostar), rabbit polyclonal somatostatin-14 (1:500, Peninsula), mouse monoclonal GAD-67 (1:500, EMD Millipore), mouse monoclonal VGAT (1:500, synaptic systems), goat polyclonal ChAT (1:500, EMD Millipore), and rabbit polyclonal NeuN (1:1000, Abcam).

10. Eukaryotic cell lines

a. State the source of each eukaryotic cell line used.	none of cell line were used
b. Describe the method of cell line authentication used.	none of cell line were used
c. Report whether the cell lines were tested for mycoplasma contamination.	none of cell line were used
d. If any of the cell lines used are listed in the database of commonly misidentified cell lines maintained by ICLAC, provide a scientific rationale for their use.	none of cell line were used

Animals and human research participants

Policy information about studies involving animals; when reporting animal research, follow the ARRIVE guidelines

11. Description of research animals

Provide details on animals and/or animal-derived materials used in the study.	In order to genetically label and manipulate chandelier cells, we crossed Nkx2.1-CreER mice (The Jackson Laboratory stock 014552) with either Rosa26-lox-stop-lox-TdTomato (Ai14) reporter (The Jackson Laboratory stock 007905) or in house derived Rosa26- lox-stop-lox-Flp (LSL-Flp) mice26. To properly identify embryonic day 17.5 (E17.5) for tamoxifen (TM) inductions, Swiss Webster females (Taconic) were housed with Nkx2.1CreER;Ai14 (het/homo) males overnight and females were checked for vaginal plug by 8-9 am the following morning. Positive plug identification was timed at E0.5. To genetically label pavalbumin positive basket cells (PVBCs), we crossed PV-Cre mice (The Jackson Laboratory stock 008069) with Ai14 reporter. The ages of animals used were ranged from postnatal 28 to 3 months, indicated in the different experiments stated in Methods. Both male and female mice were employed without distinction in all the experiments.

Policy information about studies involving human research participants

12. Description of human research participants

Describe the covariate-relevant population characteristics of the human research participants.	this study did not involve human research participants

Nature Neuroscience: doi:10.1038/nn.4624